Transworld Research Network
37/661 (2), Fort P.O., Trivandrum-695 023, Kerala, India

Thin Solid Films: Process and Applications, 2008: 281-297 ISBN: 978-81-7895-314-4
Editor: S.C.Nam

8 Recent FIB applications for TEM works of thin films

Jae-Pyoung Ahn, Kyou-Hyun Kim and Sang-Won Yoon
Advanced Analysis Center, Korea Institute of Science and Technology
Hawolkok-dong, Sungbuk-ku, Seoul 130-650, Korea

Abstract

A recent overview of a focused ion-beam (FIB) machine for the transmission electron microscope (TEM) applications is given. The emergence of FIB could dramatically reduce long sampling time required in the TEM sample preparation and could allow the expansion of analytical TEM fields in material research. In this study, we discussed two cross-sectional sample preparation methods, H bar and lift off, using FIB milling for the observation of various thin films. Also, we investigated several crucial artifacts induced by FIB milling, related to the defect generation, the precipitation of Ga ion, the crystallization or amorphization, and the change of chemical bonding. The combination of

Correspondence/Reprint request: Dr. Jae-Pyoung Ahn, Advanced Analysis Center, Korea Institute of Science and Technology, Hawolkok-dong, Sungbuk-ku, Seoul 130-650, Korea. E-mail: jpahn@kist.re.kr

FIB and TEM techniques was particularly useful for examining the interesting features which we could not see so far. Since FIB applications in TEM works have expanded for the last decade, we summarized the representative applications which have been performed by TEM after FIB milling.

1. Introduction

Transmission electron microscopy (TEM) has been routinely employed as the characterization technique of nano-scale thin films for nearly 30 years. In general, a high resolution image (HRTEM) and a selected electron diffraction (SAD) pattern in TEM are the most widely using method to perform structural analysis in the thin film. Recently line widths in the semiconductor devices narrow down in to 32 nm and it is hard to manufacture the TEM sample and to perform the complete analysis from a local interesting region.

The probe size in scanning transmission electron microscopy (STEM) narrows into 0.2 nm. It is possible to acquire the real high resolution STEM image of materials and to perform the compositional analysis at the atomic scale using energy dispersive spectroscopy (EDS) and electron energy loss spectroscopy (EELS). The thin film can include the unexpected various defects and chemical mixing at an interface of multi-layered thin films which can decide on the mechanical, physical, chemical, electrical and optical properties.

By the significant developments of analysis instruments during the last decade, the physical and chemical characteristics of thin films have been revealed. Although TEM observation gives us lots of advantages for the characterization of thin films, however, we have a strict restriction because it is still hard to make the TEM sample by the conventional method using a traditional ion-milling method. In order to overcome the problems, one begins to use the focused ion beam (FIB) to manufacture the TEM sample. The FIB with the sufficient power of 30 keV can etch samples at high speeds and can create a thin wall without mechanical breakdown. In this paper, we will discuss the TEM sample preparation method and the recent trend on FIB applications with several important artifacts and defects generated during FIB milling.

2. TEM sample preparation

2.1 History of FIB development in semiconductor and materials analysis

FIB began at 1960’s for material analyses in the field of semiconductors using sputter and implantation processes. With the founding of the ion emission from liquid metal ion sources on 1961, one could increase the brightness, the controllability and several ion species for liquid metal ion sources [1]. In particular, the liquid state of Ga at room temperature

accelerated the investigation of liquid metal ion source for the semiconductor and material research (1960~1970). In the field of semiconductors on 1973, Seligar et al. began to use a focused ion beam with liquid Ga [2, 3]. FIB acted as two roles of instrumentations and applications for material researches from 1990 and was utilized in many research fields with using the focusing columns with crossed electric and magnetic field mass separation capability [4-6].

2.2 TEM sample preparation

There are two ways in TEM sample preparation using FIB, the H bar technique [7-10] of Figure 1 and the lift-out technique of Figures 2 and 3 [5, 6]. Figure 1 shows the schematic illustration for cross-sectional TEM observation developed in the early stage of FIB sample preparation. Specimens were sectioned perpendicularly to the interesting interface using a diamond saw and polished mechanically down to the thickness of about 30 μm, which is chosen to reduce the FIB milling time and to ensure that the interesting thin film is safe from polishing damage. Using the epoxy, the polished slice (or membrane) mounted on semicircular Cu or Mo grids in Figure 1 and set-up in a FIB instrument. Since the slice should thin to 100 nm below for a TEM sample preparation, two trenches were milled away and finally the H-bar of a thin wall remains. The specimens thus prepared were examined in TEM instruments.

Recently one begins to use a Tripod-milling method to reduce more the sample thickness parallel to a conventional method. The sample can be polished down to the thickness under a few micro meters using a Tripod kit before FIB milling. It is an effective way to shorten the working time in FIB. It is also suggested a new suitable technique for making TEM specimens of small and fragile fibers and powders [9].

Figure 2 shows a schematic diagram of the lift-out technique. Recently the lift-out technique becomes a very popular method to prepare the TEM sample

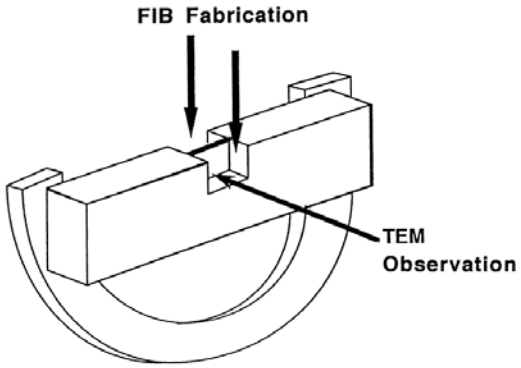

Figure 1. A schematic illustration of a sample prepared for cross-sectional TEM observation [8].

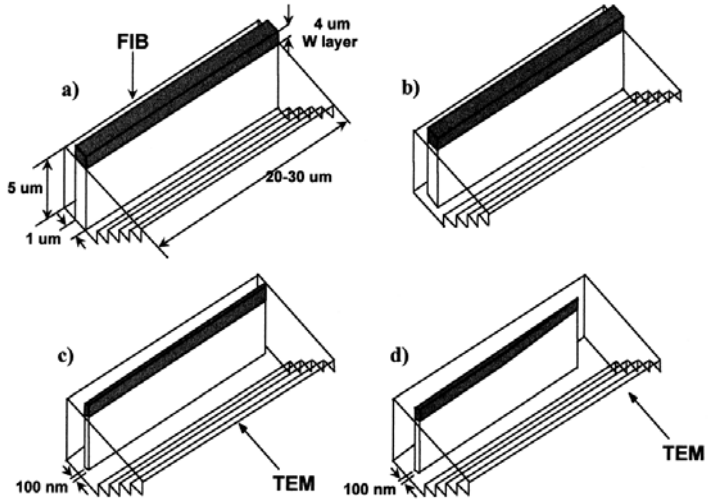

Figure 2. Schematic diagrams of the FIB lift-out technique [17]. A stair-step FIB trench is representing a right side among two trenches.

using FIB milling due to little or no initial specimen treatment [11-17]. A dark area in the Figure 2 (a) is precoated with conductive materials such as Au, C, W, or Pt to prevent the surface damage by Ga^+ sources or to eliminate the charging problems in insulating materials. In the Figure 2(b, c, and d), a slit between two trenches continues to be thinned from 1 μm to 100 nm in thickness. Here we can apply two methods in the final stage of TEM samplings, an 'external lift-out technique' and a 'wedge technique'. In the external lift-out technique, the electron transparent membrane manufactured in the Figure 2 (d) is removed from the FIB vacuum chamber and is then positioned onto carbon-coated or formvar-coated Cu TEM grids using a glass rod on a light optical microscopy. Electrostatic forces allow the membrane to be lifted out by means of the glass rod. Now we can start the meaningful TEM analysis of the specimen. Due to the low magnifications of the optical microscopy, however, it is difficult to control the position of the needle or micromanipulator around the specimen. Recently this technique is performed in FIB vacuum chamber as shown in Figure 3, showing the in situ lift-out procedure using SEM images [18]. Another specimen can be placed on the neighboring region in a Cu-grid. The membrane positioned on C film allows advantages to support the high tilting angle of about $\pm 40^o$ and EDS analysis, whilst it has disadvantages, which the lift-out specimen cannot be polished or cleaned again after positioning on the C film and it is impossible to quantify the C contents by EDS or EELS analysis.

Another useful method named the wedge technique as shown in Figure 4 is recently reported [18]. It is performed within the FIB vacuum chamber with an in-situ nanomanipulator without taking out FIB milled membrane. The images in the Figure 4 show (a) a welding process by Pt deposition between a

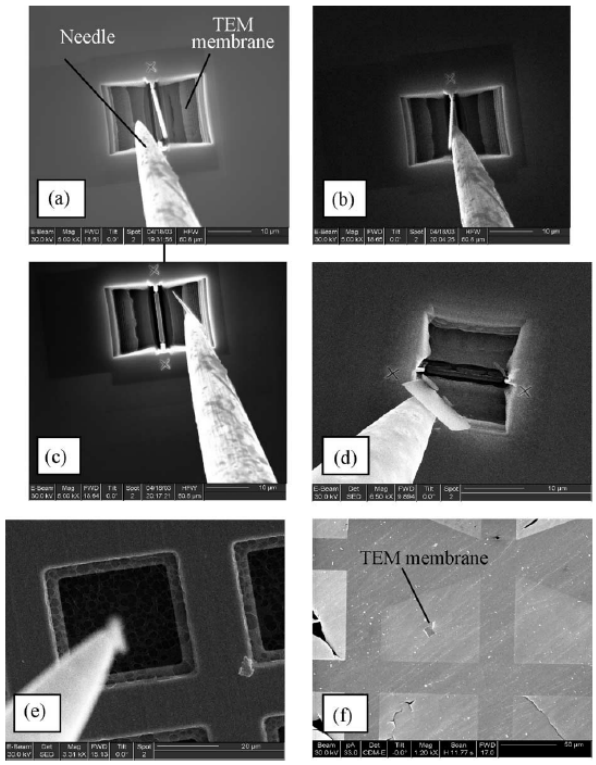

Figure 3. (a)-(f) A series of SEM images showing the in situ lift-out procedure [18]. The membrane is lifted-out by electrostatic forces (a, b), moved toward C-coated TEM mesh Cu grid by a step motor (c-e) and finally positioned on the C film (f) [18].

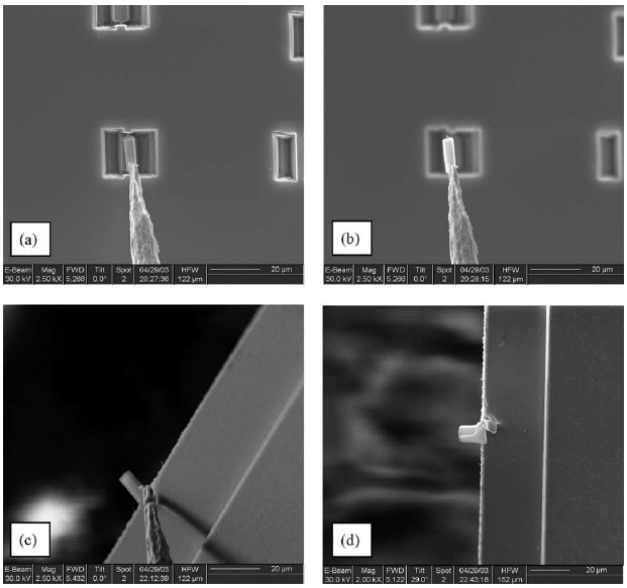

Figure 4. SEM images of (a) a cantilever shape specimen milled into the substrate with a needle Pt welded to it, (b) a wedge shaped piece of material attached to a needle raised above the sample, (c) the wedge being attached to TEM grid and (d) a wedge shape specimen attached to a grid bar into which a TEM specimen has been milled [18].

needle and a top part of the membrane, (b) a membrane raised above the sample and (c and d) the wedge attached to and welded at a Cu half grid. Finally this wedge sample mounted on a semicircular Cu grid has been milled at the low voltage FIB milling to reduce all the contaminations. The wedge technique comparing with the lift-out technique allows several advantages to ensure a high tilting angle, to make a sample without C contamination and to re-thin the membrane again.

3. Surface artifacts after FIB milling

Although FIB is widely used for TEM sample preparation, there are several crucial drawbacks such as Ga residue [19-22], Ga-induced surface damage [23-30], and Pt or C contaminations, which came from capping materials for the surface protection of samples. Ga ions can make unexpected other phases in samples. For examples, it was reported that $FeGa_3$ phase [20], particles of Ni-Ga [21], self-organized amorphization in Si crystal [22], and an amorphous layer of 24 nm in thickness at one side of thin films [31] can be formed. During the final step of FIB milling in the lift-out technique, Pt and carbon contaminations occur generally as shown in Figure 5. Figure 5 (a) shows the Pt contaminants on the thinned Fe-Al-Si alloy where dark spots indicate nanosized Pt islands. Severe contaminants are often perfectly eliminated by low voltage FIB milling. Figure 5 (b) shows the carbon contamination generated in the decomposition of organic compound after the FIB milling of Fe-Si-Al alloy. The plasma cleaning technique can often eliminate C contaminants on the sample surface. Before the plasma cleaning, the membrane contains the high contents of carbon contaminants. By the plasma cleaning for 5 min with the mixture

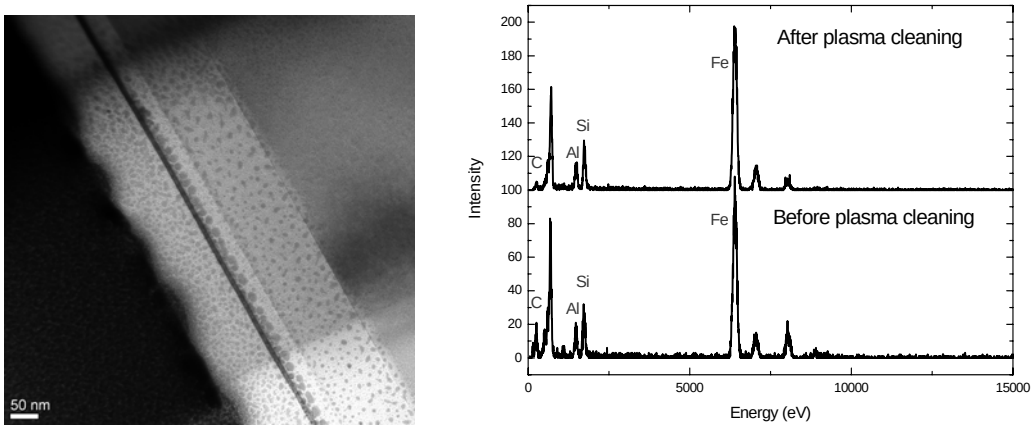

(a) (b)

Figure 5. A TEM micrograph showing Pt contaminations after FIB milling of Fe-Si-Al alloy (a) and C contamination detecting EDS acquisitions before and after plasma cleaning (b).

gas of Ar and 5% O_2, the C contaminants can be almost eliminated. In the case of the surface damage of AlAs-InAs superlattice by FIB milling, the capping layer of 60 nm by a sputter-coated gold film can protect the superlattice structure of thin films as shown in the Figure 6 [25]. If the thickness of capping materials has below 60 nm, however, the superlattice of AlAs-InAs alloy is chemically intermixed and the multi-layers are not clearly distinguished any more. It is because the energetic gallium ions collide with the atoms in the superlattice layers and chaotically displace them leading to disordering and intermixing.

TEM samples in metals or alloys can be prepared by three different methods such as jet thinning, ion milling, and FIB milling techniques. The comparison of different sampling in TEM observation was performed in Inconel 783 alloy, subjected to the standard heat treatment and prolonged isothermal exposure [33]. Figure 7, Figure 8 and Figure 9 show the TEM micrographs of the Inconel alloy [34]. All the thinning techniques of jet electro-polishing, ion milling and FIB milling were applied to the TEM sample preparation of Inconel alloy [33, 34]. As shown in the Figure 7, generally, the jet electro-polishing can produce the detailed microstructures of Inconel alloy having a large artifact of free electron transparent regions. Figure 7(a, b) shows the β phases in as-produced sample and the internal precipitation of γ′ within β phase in isothermally exposed sample. In the Figure 8, on the other hand, the ion milling technique induces artifacts on the austenitic matrix of both as-produced and exposed samples so that the morphology of γ′ phase cannot be well revealed. In the case of Figure 9, the FIB milling can cause the extensive artifacts, including surface damage and amorphous structure for the as-produced and exposed samples, rather than the ion milling. As the results above, therefore, it is not suitable to produce the TEM samples in the case of Inconel alloys using the ion and FIB milling techniques. Therefore, all above mentioned illustrations suggest that the jet electro-polishing technique is the best method to prepare the TEM sample of superalloy 783.

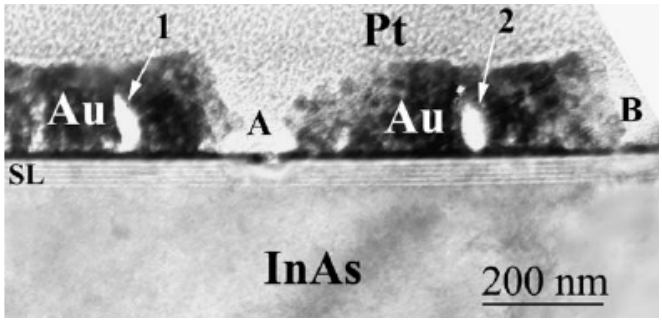

Figure 6. A cross-sectional TEM image of the gold sputter-coated protective film on an InAs substrate [32].

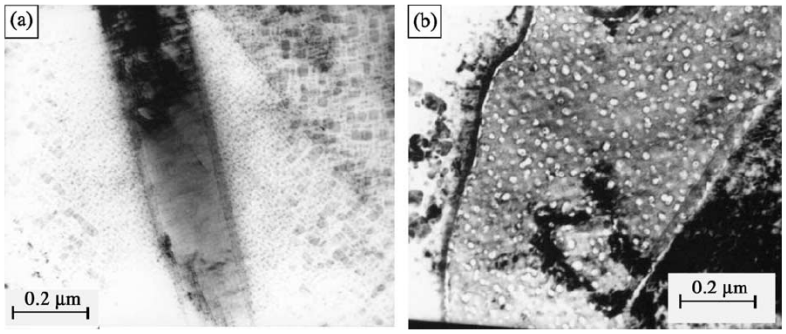

Figure 7. TEM micrographs of β phase of the Ni-based superalloy prepared by jet electro-polishing. The β phases (a) in as-produced sample and (b) in isothermally exposed sample imbedded the internal precipitation of γ′ within β phase [33].

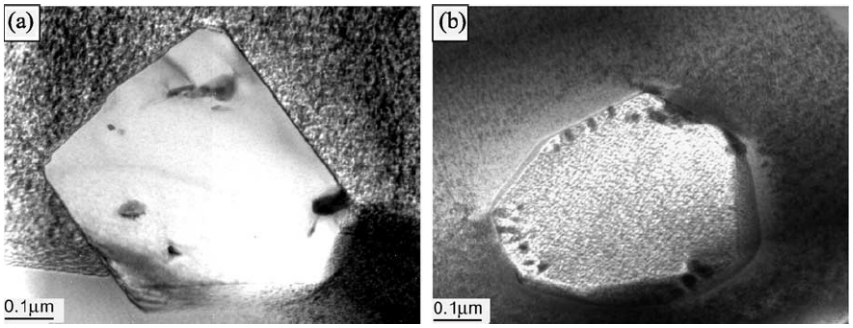

Figure 8. TEM micrographs of β phase of the Ni-based superalloy prepared by ion milling technique. The β phases (a) in as-produced sample and (b) in isothermally exposed sample imbedded the internal precipitation of large γ′ within β phase [33].

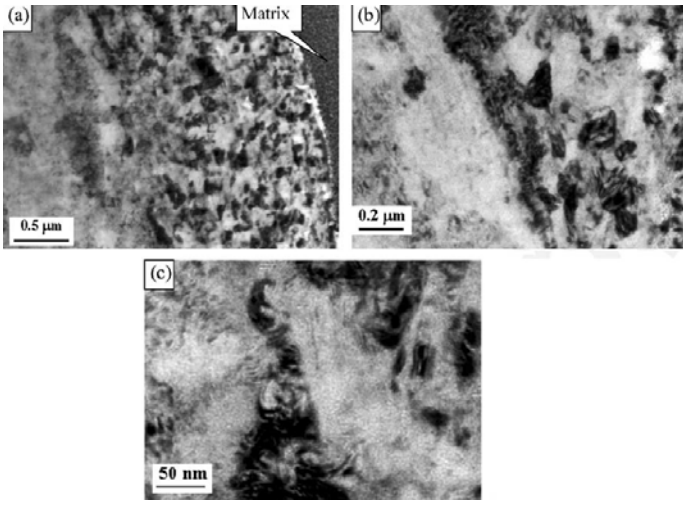

Figure 9. TEM micrographs of β phase of the Ni-based superalloy prepared by FIB milling. (a) β Phase in as-produced sample; (b) β phase in isothermally exposed sample; (c) high magnification view of (b) [33].

The FIB milling can induce the destruction of chemical bonds due to the bombardment of Ga^+ ion. A typical example is shown in Figure 10, which is (a) a STEM HAADF (high angular annular dark field) micrograph of a diamond thin film prepared by FIB and (b) EELS spectra acquired from each different region marked on Figure 10(a). The diamond thin film of 1 μm in thickness was manufactured by DC magnetron sputtering and its cross-sectional TEM sample was prepared by FIB operated under a condition of the acceleration voltage of 30 keV and the beam current of 65 nA. An EELS spectrum generally includes the information of the chemical bonding. We performed the EELS measurements for the chemical analysis of FIB-milled TEM sample. The STEM HAADF image shows the diamond grains with about 5~10 nm in diameter. The carbon K-edge EELS spectrum clearly shows that the thin film consists of the chemical bonding with diamond structure [35]. We tried to investigate the FIB milling effects by measured a EELS spectrum, showing the thickness effects on the chemical bonding as shown in the Figure 10(b). At the thinnest region marked as number 1, the carbon K-edge EELS spectrum indicates a typical amorphous carbon which consists of sp^2 and sp^3 bonding, while the regions of numbers 2 to 6 show the diamond bonding of only sp^3. The observation of sp^2 at the number 1 means that the diamond transferred to the amorphous structure due to the surface damage by FIB milling. Since FIB milled sample has wedge shape, thinner regions generally contains the relatively higher defects than thicker those. Therefore, the thinner region reveals surface properties involving an amorphizing transformation. The destruction of chemical structure by FIB milling was distributed in the range of a few tens to hundreds nanometer in the case of diamond thin film. It is clear that such a phenomenon during TEM sample preparation by FIB milling is very serious problems for the chemical analysis using EELS applications, but unfortunately it does not seem to be solved so far, in spite of using the low voltage FIB milling method.

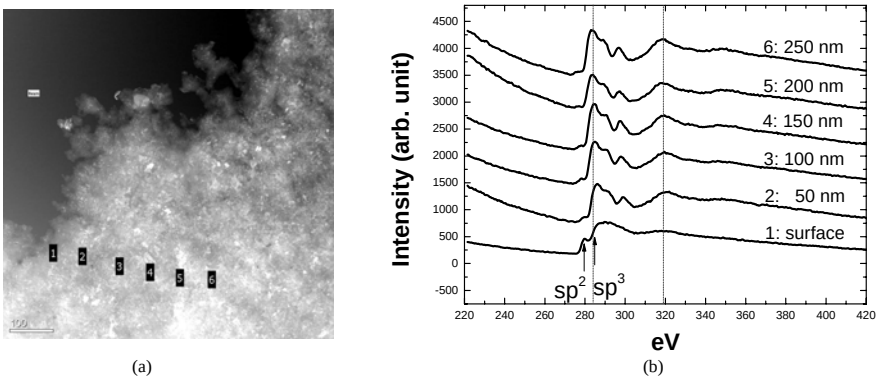

(a) (b)

Figure 10. (a) A STEM HAADF micrograph of a diamond thin film prepared by FIB milling and (b) EELS spectra acquired from each different region marked on Figure 7(a).

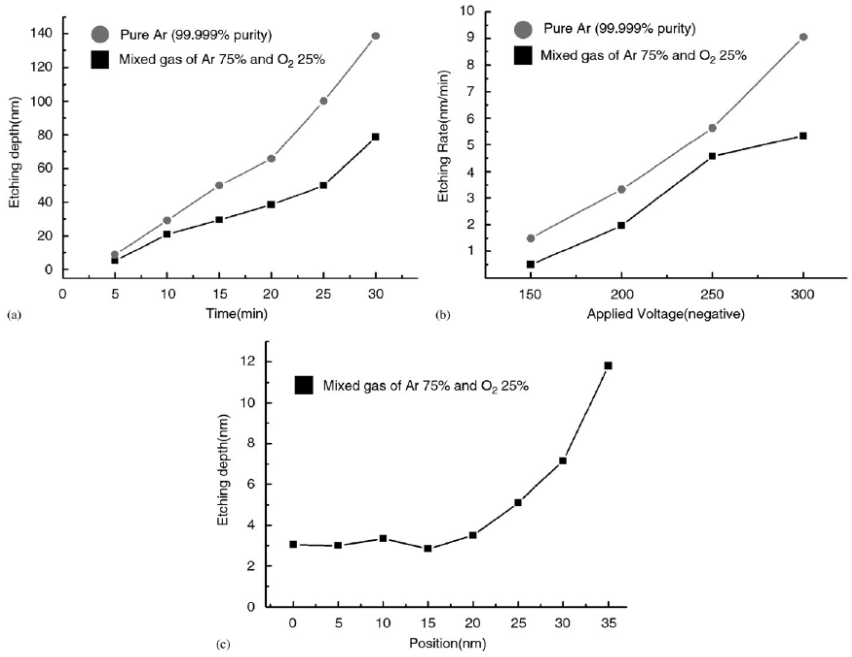

Fig. 2. Plasma etching rate of SiO_2 as a function of (a) time at a bias voltage of 200 V, (b) bias voltage with a fixed etching time of 15 min and (c) the variation of the etch rate with different positions at a bias voltage of 150 V.

Figure 11. Plasma etching rate of SiO_2 as a function of (a) time at a bias voltage of 200 V, (b) bias voltage with a fixed etching time of 15 min and (c) the variation of the etch rate with different positions at a bias voltage of 150 V [23].

In order to remove the artifacts induced by the Ga ion source with high energy, by the way, the low energy ion milling (gentle mill or low voltage ion milling) is an effective method [32, 36, 37]. However, there are some practical problems by a complicated geometry and a big difference in roughness. A simple and effective method [23] was suggested to remove the surface damage using plasma cleaner, which is commonly used in TEM laboratories to reduce the hydro-carbon contamination of samples under the electron beam [38-40]. The proposed technique could be applied to any sample made by either FIB or energetic ion beams with a controllable etching rate as shown in the Figure 11. For example, the removal rates of SiO_2 with experimental conditions of plasma cleaner were reported. The removal rate of thin SiO_2 film became 4.1 nm/min for pure argon gas and dropped to 2.1 nm/min for the mixture gas of Ar and O_2. It is interest that the technique can be used to reduce the thickness of surface artifacts coming from ion milling or natural oxidation.

4. Recent FIB applications

FIB has been successfully applied to TEM sample preparations from extremely small features, various composite materials and complicated geometries. FIB is used in the fields of ion implantations [41], surface reactions [42-45], interfaces by coatings or depositions [46-51], defects just

below the surface [52-54], in-situ behaviors [55], textured orientation [56, 57], and 3D observations [58], and nano patternings [59-63]. In this session, we will briefly touch the distinguishable concepts in each field.

Figure 12 shows the local compositional analysis of SiC microstructures inside silicon formed by carbon implantations under the acceleration voltage of 1.5 MeV. It is demonstrated that the combination of FIB sampling and EFTEM observations provides an ideal technique to characterize the local structure and compositional analysis of the SiC sublayer with an adequate spatial resolution. From the TEM specimens made by FIB milling, they could compare the C contents and crystal structures of the SiC microstructure formed under various dose levels and temperatures, leading to amorphization even at target temperatures as high as 600^{o}C.

Figure 13 and Figure 14 show the cross-sectional investigation of isolated diamond particles grown on Si substrates [45]. It is the most typical example of FIB applications. Figure 13 shows the optical micrograph which indicates the crystallographic direction cut by FIB. The FIB milling was performed to carve out a thin diamond cross section precisely through the center. From the FIB-milled specimen, they could observe a cross-sectional structure from the nucleation center to the growth edge as shown in Figure 14.

Figure 14 shows (a) a whole cross-sectional, a nice TEM micrograph, and (b) a schematic drawing indicating the crystallographic orientations. The diamond particle has generally high crystallinity and the growth behavior depends on the defects. In order to recognize the exact growth mechanism of

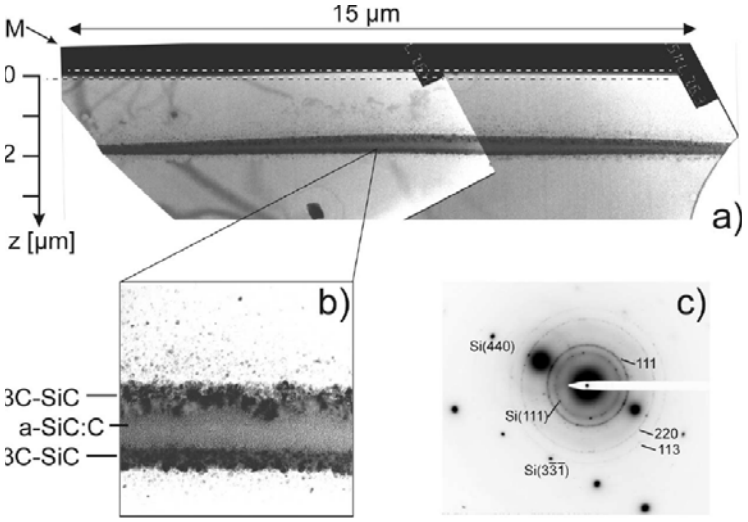

Figure 12. (a) XTEM bright-field images showing a cross-section of the buried SiC line, (b) detail of the SiC structure at the centre of the line, and (c) selected area diffraction pattern showing the poly-rings of SiC and of poly-Si, in addition to matrix spots of Si [60]. The dashed rectangular lines are to highlight the surface swelling and 'M' denotes the metal coating.

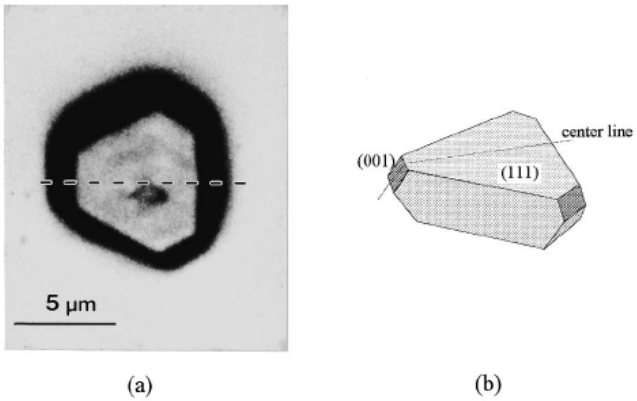

Figure 13. (a) Optical micrograph of (111)-oriented cubo-octahedral diamond particle and (b) its schematic drawing. The nucleation site was assumed to be at the center of the particle [45].

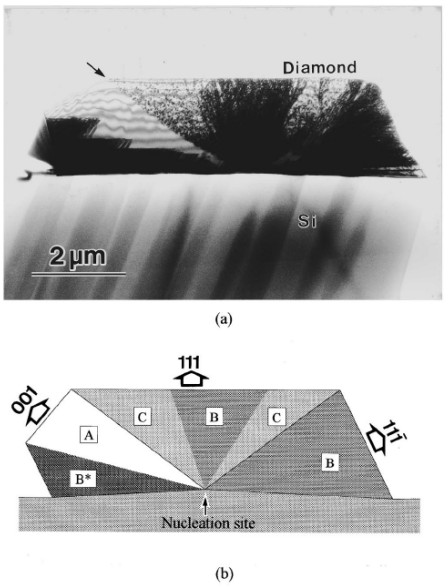

Figure 14. (a) Whole cross-sectional TEM view of the diamond (-1-10) plane and (b) the schematic drawing indicating the crystallographic orientations. The cross section was fabricated by FIB micromachining at the center of the particle. The outline of the specimen is made to wavy due to the erosion by the FIB. Note the configuration of the defects (A: defect-free region; B and B*: stacking fault region; C: dislocation loop region and slight curvature of the interface) [45].

diamond particles, therefore, we can select the direction of TEM sampling. Figure 14 has clearly revealed that the growth defects of diamonds are closely connected with the growth orientation. For example, the area grown in the [001] direction is of defect-free crystal and the area grown in the [111] direction contains a lot of defects. It is speculated to be due to the difference

between the properties of the [100] and [111] surfaces. In conclusion, the growth mechanism of the isolated diamond particles was found to be related to the orientation relationship between growth orientations and internal defects of the diamond particle from the cross-sectional TEM sample prepared by FIB milling. It is expected that the method above can be widely used in the crystallographical interpretation on the growth mechanism of particles grown on the substrate.

The FIB has been generally used for the structure analysis of various coating layers: for example, TiN coatings on steel substrates, oxide layers of a frication stir welded Al alloy, each interface of yttria-stabilized zirconia (YSZ) multi-coating layers, a thin film transistors on glass substrates, and so on.

Hard coating layers are evaluated by several techniques such as adhesion, scratch, abrasive, and indentation tests. According to reducing the coating thickness as a trend, recently, a nanoindentaion technique comes to be more popular for effective evaluations. Figure 15 shows the TEM micrographs of TiN hard coating at the indented region [50]. The TEM sampling by FIB milling was performed at the cross section parallel to a pressing direction. In the Figure 15, we can see a macro crack with the length of 5 μm. Also, it is clearly shown in the Figure 15 (b) that the TiN coating layer has deformed by shear sliding of the grains at the columnar grain boundaries, which was represented by multi-shear steps, marked S, adjacent to the macro crack. Here, cracks running along the columnar grain boundaries can be clearly observed. Transgranular cracks, marked T, across the columnar grains can be observed in the Figure 15 (b, c), which is taken from an area close to the edge of the indent. Nobody has shown such a TEM observation so far. It is possible to use the FIB milling technique

Surface modifications in optoelectronics and semiconductor technology have been increasingly processed for the realization of particular properties. These technologies give rise to structural modulation, chemical mixing and phase transformation in local area. Because of small features of nanometer under, however, the TEM sampling process becomes important and challenging issues. Lithium niobates used in optoelectronics with periodic and repeatable features is manufactured for the nonlinear optical characteristics. Figure 16 (a) shows the nanoscale surface and subsurface defects induced in lithium niobate ($LiNbO_3$) by a femtosecond laser. Around these layers, the semicircular contour of the locally ablated sample with a diameter of about 2 μm, related to the laser pulse, is seen. A semicircular layer with a gray contrast just below the contour of 100 nm was formed by laser works. It was proven by selected area electron (SAD) diffraction in (b) that the layer was amorphous, comparing with that of a substrate which shows a crystal SAD pattern in (c). From EDS profiles of oxygen and niobium at each region, it is observed that

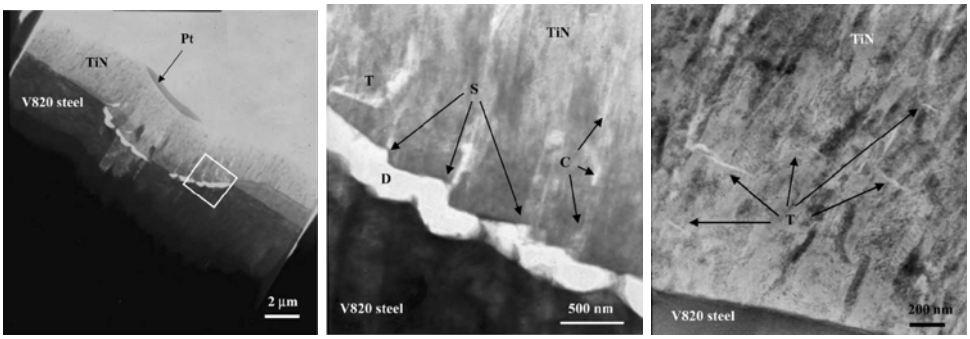

Figure 15. (a) Bight field TEM image of the LVEB TiN coating following nanoindentation at a load of 500 mN using a spherical indenter of 5 μ radius. (b) Bright field TEM image, at higher magnification, of the area indicated by the white square, shown in (a). (c) Bright field TEM image of the transgranular cracks at higher magnification from the indented region shown in (a) [50].

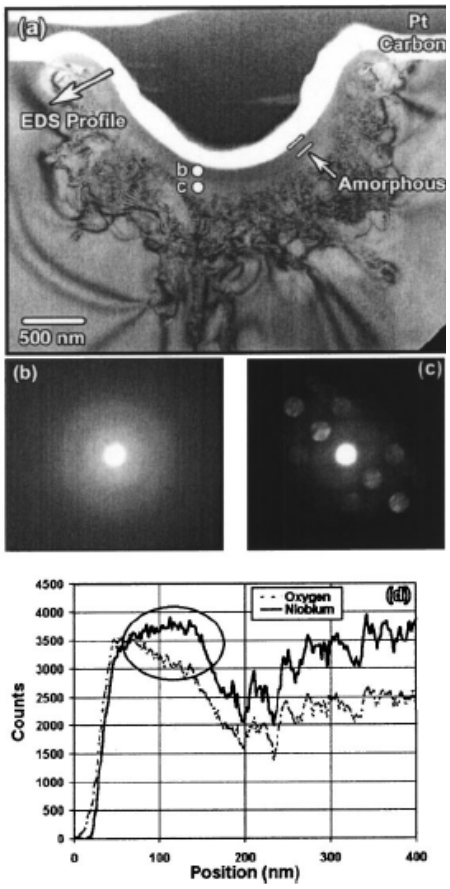

Figure 16. (a) Bright-field TEM micrograph of the nanoscale surface and subsurface defects induced in lithium niobate ($LiNbO_3$) by a femtosecond laser, (b and c) transmission electron diffraction patterns from the areas, and (d) EDS profile. The circle denotes the area where oxygen deficiency is observed [54].

the first 100 nm of the line profile shows the evidence of oxygen deficiency, i.e., the amorphous region has a gradient in oxygen content from substoichiometric towards stoichiometric at the start of the crystalline region. These observations can predict that picosecond ablation of $LiNbO_3$ might remove oxygen and lithium from the crystal [54].

5. Summary

With the occurrence and development of FIB instrument, it is clear that the FIB becomes a very useful tool to make the TEM sample from various and complicate specimens. However, it is required that we have to understand and to avoid lots of artifacts occurring by the high energy milling of FIB instrument. Also, the TEM samples prepared by FIB milling are often not good enough for EELS works even after the FIB milling with low energy. Considering the recent developing rate of FIB instruments, nevertheless, it is expected that the disadvantages of FIB milling in all the TEM works containing EELS applications can be overcome in the near future.

6. References

1. E.C. Jones, P.L. Krohn, Journal of Endocrinology 21/4 (1961) 469.
2. R.L. Seliger, W.P. Fleming, J. Vac. Sci. Technol. 10/6 (1973) 1127.
3. R.L. Seliger, W.P. Fleming, J Appl Phys 45/3 (1974) 1416.
4. R.L. Seliger, J.W. Ward, V. Wang, R.L. Kubena, Appl Phys Lett 34/5 (1979) 310.
5. V. Wang, J.W. Ward, R.L. Seliger, Journal of Vacuum Science & Technology 19/4 (1981) 1158.
6. T. Shiokawa, P.H. Kim, K. Toyoda, S. Namba, T. Matsui, K. Gamo, Journal of Vacuum Science & Technology B 1/4 (1983) 1117.
7. R. Hull, D. Bahnck, F.A. Stevie, L.A. Koszi, S.N.G. Chu, Appl Phys Lett 62/26 (1993) 3408.
8. K. Kuroda, M. Takahashi, T. Kato, H. Saka, S. Tsuji, Thin Solid Films 319/1-2 (1998) 92.
9. J. Li, T. Malis, S. Dionne, Materials Characterization 57/1 (2006) 64.
10. R. Patterson, D. Mayer, L. Weaver, M. Phaneuf, Proceeding of Microscopy and Microanalysis 8 (2002) 566.
11. M.H.F. Overwijk, F.C. Vandenheuvel, C.W.T. Bullelieuwma, Journal of Vacuum Science & Technology B 11/6 (1993) 2021.
12. A.J. Leslie, K.L. Pey, K.S. Sim, M.T.F. Beh, G.P. Goh, 21st International Symposium for Testing and Failure Analysis (1995) 353.
13. L.R. Herlinger, S. Chevacharoenkul, D.C. Erwin, 22nd International Symposium for Testing and Failure Analysis (1996) 199.
14. F.A. Stevie, S.W. Downey, S. Brown, T. Shofner, M. Decker, T. Dingle, L. Christman, Microscopy Microanalysis 4 (1998) 650.
15. T.T. Sheng, G.P. Goh, C.H. Tung, J.L.F. Wang, J.K. Cheng, Proceedings of the International Symposium on the Physical and Failure Analysis of Integrated Circuits, 1997.

16. L.A. Giannuzzi, J.L. Drown, S.R. Brown, R.B. Irwin, F.A. Stevie, Materials Research Society Symposium Proceedings, Materials Research Society, 1997.
17. L.A. Giannuzzi, F.A. Stevie, Micron 30/3 (1999) 197.
18. R.M. Langford, C. Clinton, Micron 35/7 (2004) 607.
19. D.S. Ko, Y.M. Park, S.D. Kim, Y.W. Kim, Ultramicroscopy 107/4-5 (2007) 368.
20. J.S. Yu, J.L. Liu, J.X. Zhang, J.S. Wu, Materials Letters 60/2 (2006) 206.
21. M. Tanaka, K. Furuya, T. Saito, Nuclear Instruments & Methods in Physics Research Section B-Beam Interactions with Materials and Atoms 127 (1997) 98.
22. Y. Huang, D.J.H. Cockayne, C. Marsh, J.M. Titchmarsh, A.K. Petford-Long, Applied Surface Science 252/5 (2005) 1954.
23. M. Tanaka, K. Furuya, T. Saito, Thin Solid Films 319/1-2 (1998) 101.
24. J.Y. Dai, S.F. Tee, C.L. Tay, Z.G. Song, S. Ansari, E. Er, S. Redkar, Microelectronics Journal 32/3 (2001) 221.
25. S. Rubanov, P.R. Munroe, Materials Letters 57/15 (2003) 2238.
26. S. Rubanov, P.R. Munroe, Micron 35/7 (2004) 549.
27. C.R. Hutchinson, R.E. Hackenberg, G.J. Shiflet, Ultramicroscopy 94/1 (2003) 37.
28. G.B. Thompson, M.K. Miller, H.L. Fraser, Ultramicroscopy 100/1-2 (2004) 25.
29. G.A. Botton, M.W. Phaneuf, Micron 30/2 (1999) 109.
30. Z. Czigany, J. Neidhardt, I.F. Brunell, L. Hultman, Ultramicroscopy 94/3-4 (2003) 163.
31. J.P. McCaffrey, M.W. Phaneuf, L.D. Madsen, Ultramicroscopy 87/3 (2001) 97.
32. A. Barna, B. Pecz, M. Menyhard, Ultramicroscopy 70/3 (1998) 161.
33. L.Z. Ma, Micron 35/4 (2004) 273.
34. G. Appa Rao, M. Srinivas, D.S. Sarma, Materials Science and Engineering A 383 (2004) 201.
35. K. Okada, K. Kimoto, S. Komatsu, S. Matsumoto, J Appl Phys 93/5 (2003) 3120.
36. A. Barna, B. Pecz, M. Menyhard, Micron 30/3 (1999) 267.
37. Y.W. Kim, Metals and Materials International 7/5 (2001) 499.
38. T.C. Isabell, P.E. Fischione, C. O'Keefe, M.U. Guruz, V.P. Dravid, Microscopy and Microanalysis 5/2 (1999) 126.
39. T.C. Isabell, P.E. Fischione, Mat. Res. Soc. Symp., 1998, p. 31.
40. P. Fischione, J. Ringnalda, Y. Feng, T. Krekels, M. Hayles, J. Colijn, M. Mills, J. Wiezorek, Mat. Res. Soc. Symp. 480 (1997) 225.
41. J.K.N. Lindner, S. Kubsky, A. Schertel, Materials Science and Engineering B-Solid State Materials for Advanced Technology 102/1-3 (2003) 70.
42. A. Imai, C. Kamiya, Y. Fujimoto, F. Okuyama, Surface Science 461/1-3 (2000) L515.
43. M. Tarutani, Y. Shimato, Y. Takai, R. Shimizu, Appl Phys Lett 67/5 (1995) 632.
44. Y.S. Sato, F. Yamashita, Y. Sugiura, S.H.C. Park, H. Kokawa, Scripta Mater 50/3 (2004) 365.
45. M.J. Lindsay, M.G. Blackford, D.J. Attard, V. Luca, M. Skyllas-Kazacos, C.S. Griffith, Electrochimica Acta in press (2007).
46. J.M. Cairney, S.G. Harris, P.R. Munroe, E.D. Doyle, Surface & Coatings Technology 183/2-3 (2004) 239.
47. T. Kato, M.H. Hong, K. Nunome, K. Sasaki, K. Kuroda, H. Saka, Thin Solid Films 319/1-2 (1998) 132.
48. L.W. Ma, J.M. Cairney, M. Hoffman, P.R. Munroe, Surface & Coatings Technology 192/1 (2005) 11.

49. T. Kato, K. Matsumoto, H. Matsubara, Y. Ishiwata, H. Saka, T. Hirayama, Y. Ikuhara, Surface & Coatings Technology 194/1 (2005) 16.
50. K. Tsujimoto, S. Tsuji, K. Kuroda, H. Saka, Thin Solid Films 319/1-2 (1998) 106.
51. F. Perez-Willard, D. Wolde-Giorgis, T. Al-Kassab, G.A. Lopez, E.J. Mittemeijer, R. Kirchheim, D. Gerthsen, Micron In Press (2007)
52. E.A. Stach, V. Radmilovic, D. Deshpande, A. Malshe, D. Alexander, D. Doerr, Appl Phys Lett 83/21 (2003) 4420.
53. H. Saka, S. Abe, Mat Sci Eng a-Struct 234 (1997) 552.
54. U. Muhle, A. Wiesner, S. Schray, Microelectronics and Reliability 38/6-8 (1998) 895.
55. C. Petersen, A. Lasagni, C. Holzapfel, C. Daniel, F. Mucklich, M. Veith, Applied Surface Science In Press (2007).
56. E. Eiper, J. Keckes, K.J. Martinschitz, I. Zizak, M. Cabie, G. Dehm, Acta Mater 55/6 (2007) 1941.
57. Y.H. Lee, I.C. Leu, M.T. Wu, J.H. Yen, K.Z. Fung, J Alloy Compd 427/1-2 (2007) 213.
58. A.E.M. De Veirman, Materials Science and Engineering B 102/1-3 (2003) 63.
59. A.Y. Toporov, R.M. Langford, A.K. Petford-Long, Appl Phys Lett 77/19 (2000) 3063.
60. Y. Lei, W.P. Cai, G. Wilde, Progress in Materials Science 52/4 (2007) 465.
61. S. Frabboni, G.C. Gazzadi, A. Spessot, Physica E: Low-dimensional Systems and Nanostructures 37/1-2 (2007) 265.
62. S. Matsui, Nuclear Instruments and Methods in Physics Research Section B: Beam Interactions with Materials and Atoms 257/1-2 (2007) 758.
63. K. Arshak, M. Mihov, S. Nakahara, A. Arshak, D. McDonagh, Microelectron Eng 78-79 (2005) 39.